Durations and Separations of Equatorial Plasma Depletions Observed by the Planar Langmuir Probe Onboard the C/NOFS Satellite

Emanoel Costa[1], Patrick A. Roddy[2], John O. Ballenthin[2], and Keith M. Groves[3]

[1]Centro de Estudos de Telecomunicações, Pontifícia Universidade Católica do Rio de Janeiro,
Rua Marquês de São Vicente 225, 22451-900 Rio de Janeiro RJ Brazil, e-mail: epoc@cetuc.puc-rio.br

[2]Space Vehicles Directorate, Air Force Research Laboratory, Kirtland Air Force Base, NM, U.S.A., e-mails:
patrick.roddy@us.af.mil, ballenthin@us.af.mil

[3]Institute for Scientific Research, Boston College, Chestnut Hill, MA, U.S.A., e-mail:keith.groves@bc.edu

This paper was prepared for presentation during the 15th International Congress of the Brazilian Geophysical Society held in Rio de Janeiro, Brazil, 31 July to 3 August, 2017.

Abstract

The present contribution provides statistical descriptions of durations and separations of equatorial plasma bubbles detected by the Planar Langmuir Probe onboard the C/NOFS satellite, considering their dependence on the solar activity.

Introduction

The analysis of *in situ* measurements of ionospheric electron density made it possible to establish the climatology of the occurrence of equatorial plasma bubbles, considering several geophysical factors [1] – [4]. It is also known that the longitudinal size and depths of plasma bubbles can reach several hundred kilometers and three orders of magnitude, respectively [5]. However, more detailed information on the last two aspects of equatorial plasma bubbles, as well as on their separations, is not so widely available. Yet, such information could be useful for planning and operating communication and navigation systems, as well as for fine-tuning computer simulation tools of ionospheric plasma instability processes. The objective of the present contribution is to provide statistical descriptions of durations and separations of equatorial plasma bubbles.

In the following section, the Planar Langmuir Probe (PLP) data and its pre-processing will be described. Next, the statistics of durations and separations of different depletion depths will be presented and discussed, considering their dependence on the solar activity. The main conclusions from the analysis will be listed in the final section.

Data description and pre-processing

PLP C/NOFS data are available to the present work in individual daily files with 1-Hz resolution. Each 1-s record associates the Universal Time (s) to the corresponding average ion density N_i (ions/cm^3), standard deviation of the ion density δN_i (ions/cm^3), ratio $\delta N_i/N_i$, as well as satellite latitude (degrees), longitude (degrees), and altitude (km) in WGS84 coordinates. The values N_i and δN_i are obtained from the high resolution data (sampled at 512 Hz during evening hours) for the corresponding second. Figure 1 displays an example of PLP data acquired during a single orbit (between consecutive crossings of the geographic equator) centered on local solar midnight. Its top panel shows the one-second (green) and one-minute (black) average ion densities according to the left vertical axis. This panel also shows the altitude of the satellite, based on the right vertical axis (blue, with eclipse indicated by the heavily dotted line). The central panel shows spectrograms of the full 512 Hz data converted into distance units (left vertical axis), with spectral power given in fixed relative units. The bottom panel represents the ground track of the satellite (red, heavily dotted during the eclipse), together with the magnetic equator (green).

The results to be discussed in the next sections will be based on a level-crossing analysis of the ratio *Ni/Ns*, where *Ns* (ions/cm^3) is a tight upper envelope to the average ion density *Ni*, representing the background ion density. In principle, *Ns* could have been determined by a running average or low-pass filter version of *Ni*. However, both procedures would tend to follow *Ni* depletions (possibly in an attenuated fashion, depending on length of the running average or on the filter parameters). To minimize these effects, *Ns* was alternatively determined by a three-step procedure, partially based on the ratio $\delta N_i/N_i$. As an aide to the description of this procedure, Figure 2 displays C/NOFS PLP data from the disturbed section of orbit 25640, between 22:37 UT (81420 s) and 22:52 UT (82320 s). The green curve (left vertical axis) represents the one-second average ion density *Ni* (ions/cm^3). The blue curve (right vertical axis) represents

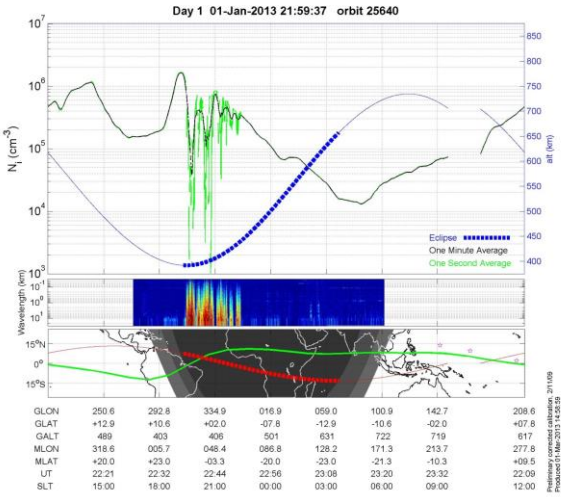

Figure 1. Data from the C/NOFS satellite orbit 25640, on 01 January 2013. (top) One-minute (black line) and one-second (green line) average ion density, with respect to the left vertical axis; and satellite altitude (blue line), according to the right vertical axis. (middle) Power spectral density from the 512 Hz PLP data. (bottom) Map with the C/NOFS satellite ground track (red) and geomagnetic equator (green). The thick dotted lines indicate the eclipse period of the C/NOFS satellite.

the ratio $\delta N_i/Ni$ between the standard deviation of the ion density δN_i (ions/cm^3) and the average ion density *Ni* (ions/cm^3).

The results to be discussed in the next sections will be based on a level-crossing analysis of the ratio *Ni/Ns*, where *Ns* (ions/cm^3) is a tight upper envelope to the average ion density *Ni*, representing the background ion density. In principle, *Ns* could have been determined by a running average or low-pass filter version of *Ni*. However, both procedures would tend to follow *Ni* depletions (possibly in an attenuated fashion, depending on length of the running average or on the filter parameters). To minimize these effects, *Ns* was alternatively determined by a three-step procedure, partially based on the ratio $\delta N_i/N_i$. As an aide to the description of this procedure, Figure 2 displays C/NOFS PLP data from the disturbed section of orbit 25640, between 22:37 UT (81420 s) and 22:52 UT (82320 s). The green curve (left vertical axis) represents the one-second average ion density *Ni* (ions/cm^3). The blue curve (right vertical axis) represents the ratio $\delta N_i/Ni$ between the standard deviation of the ion density δN_i (ions/cm^3) and the average ion density *Ni* (ions/cm^3).

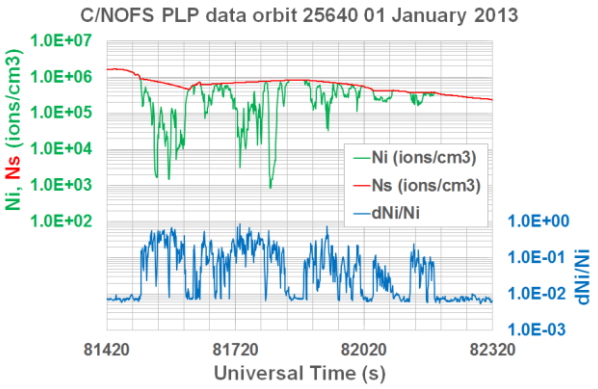

Figure 2. C/NOFS PLP data from the disturbed section of orbit 25640, between 22:37 UT (81420 s) and 22:52 UT (82320 s). The green curve (left vertical axis) represents the one-second average ion density Ni (ions/cm^3). The blue curve (right vertical axis) represents the ratio $\delta N_i/Ni$ between the standard deviation of the ion density δN_i (ions/cm^3) and the average ion density Ni (ions/cm^3). The red curve (left vertical axis) indicates the tight upper envelope Ns (ions/cm^3) to the average ion density Ni curve, representing the background ion density.

Note in Figure 2 that ratio $\delta N_i/Ni$ is relatively flat (and obviously small) outside plasma bubbles. Thus, *Ns* is initially equated to *Ni* whenever the corresponding ratio $\delta N_i/Ni$ is less than a threshold (0.009). The undefined values *Ns* are obtained by linear interpolation between the *Ni* values at the extremes of the gap intervals. The second step in the procedure was designed to eliminate fast variations observed in the provisional *Ns* curve resulting from the first step, as follows. If the ratio $Ns(j+j_o)/Ns(j)$ (for $j = 1$ and a fixed value for j_o) is less than another threshold, then all the *Ns* values in the batch ($j < k \leq j+j_o$) are replaced by *Ns(j)*. When applied, this step resembles a *max hold* algorithm (with $j_o = 30$ and the threshold equal to 0.5 in the present study). Regardless of the decision, the current value of the index *j* is incremented by j_o and the process is repeated for all batches. In the last step of the procedure, the resulting value *Ns(j)* is replaced by *Ni(j)* whenever $Ns(j) < Ni(j)$. It should be noticed that the above procedure generally incorporates density enhancements into the background ion density, with no detrimental impact on the analysis of plasma depletions [6], [7].

The results from the application of the above pre-processing to the disturbed section of orbit 25640 are represented by the red curve (left vertical axis) of Figure 2. The corresponding curve log(*Ni/Ns*) that will be used in the level-crossing analysis, which is non-positive, indicating that *Ns* indeed is a tight upper envelope to the average ion density *Ni*, is displayed in Figure 3.

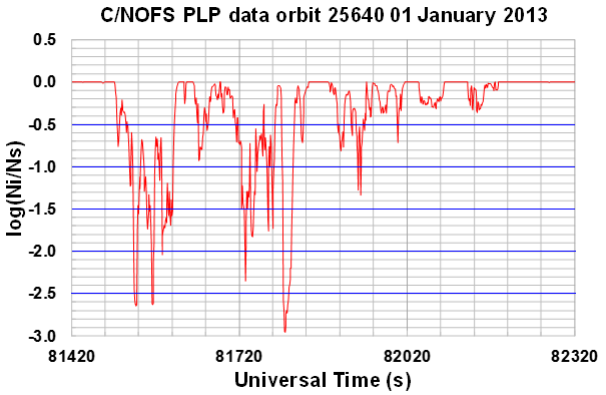

Figure 3. Red curve log(Ni/Ns) corresponding to the C/NOFS PLP data from the disturbed section of orbit 25640, between 22:37 UT (81420 s) and 22:52 UT (82320 s). The Ni and Ns values are represented by the green and red curves of Figure 2. The levels selected for analysis are indicated by the five blue horizontal lines.

As an additional indication that the above pre-processing successfully determined the desired representation of the environment density, Figure 4 displays histograms of log(*Ni/Ns*) for two different years (01 October 2008 to 30 September 2009 and 05 June 2012 to 04 June 2013) of C/NOFS PLP ion density data. The first data set corresponds to solar minimum conditions and the second one is as close to solar maximum conditions of solar cycle 24 as possible at the time of the analysis. As desired, the histograms show the absence of samples with log(*Ni/Ns*) > 0 (*Ni* > *Ns*). It is also observed that the histograms of log(*Ni/Ns*) for the two very different years remain very close to each other for abscissas as low as -2 (depletions by two orders of magnitude with respect to the background density). This is to be expected, since *Ni* and *Ns* are both small during solar minimum conditions with respect to their corresponding solar maximum values. Thus, the ratio *Ni/Ns* tends to become relatively independent from solar activity. A similar behavior is observed in the upper panel of Figure 5, which displays the histograms of log(δ*Ni/Ni*), which also involves the ratio of two variables, for the same years. Indeed, for log(δ*Ni/Ni*) > -2 (that is, for 1 % irregularities or stronger), the histograms corresponding to the two years differ by a factor of four at most. On the other hand, the histograms of log(δ*Ni*) (the un-normalized value of the standard deviation of the ion density) displayed by the lower panel of Figure 5, indicate a 100-fold increase in the number of samples with $\delta Ni = 10^5$ ions/cm^3 due to the difference between the effects of solar minimum and maximum conditions on the low-latitude ionosphere. The above remarks on the differences between studies of normalized or un-normalized ionospheric densities are aligned with previous observations by *Huang et al.* [8] and *Costa et al.* [9]. These authors also agree that un-normalized patterns of δNi are more consistent with those of ionospheric scintillation. However, it should be clear that the present work focuses on plasma depletions, relative to a baseline defined by the background ion density. Therefore, log(*Ni/Ns*) is the parameter to be investigated.

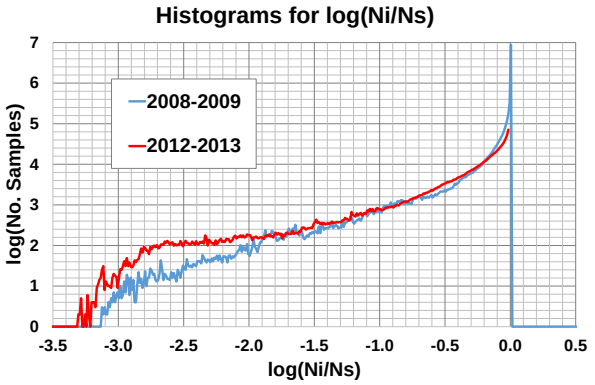

Figure 4. Histograms of log(Ni/Ns) for two different years (01 October 2008 to 30 September 2009 and 05 June 2012 to 04 June 2013) of C/NOFS PLP ion density data. The first data set corresponds to solar minimum conditions and the second one is as close to solar maximum conditions of solar cycle 24 as possible at the time of the analysis.

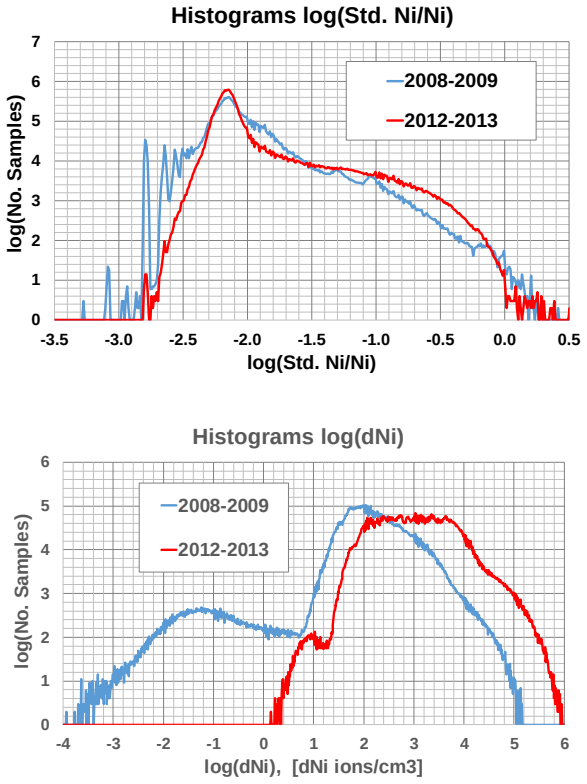

Figure 5. Histograms of log(δNi/Ni) (upper panel) and log(δNi) (lower panel) for two different years (01 October 2008 to 30 September 2009 and 05 June 2012 to 04 June 2013) of C/NOFS PLP ion density data. The first year corresponds to solar minimum conditions and the second one is as close to solar maximum conditions of solar cycle 24 as possible at the time of the analysis.

Statistics of Durations and Separations of Different Depletion Depths

Five different depletion depths were selected for analysis, as indicated by the blue horizontal lines of Figure 3: log(*Ni/Ns*) = -0.5, -1.0, -1.5, -2.0, and -2.5. The depletion interval is defined by the time interval between consecutive crossings of the selected log(*Ni/Ns*) level, the first with a negative slope and the second with a positive slope. During a depletion interval, log(*Ni/Ns*) is below the selected level Figure 3 shows three depletions with log(*Ni/Ns*) < -2.5. The durations of the first and third depletions are approximately 8 s and 15 s (while the second one is considerably shorter). A separation interval is defined by the time interval between consecutive crossings of the selected log(*Ni/Ns*) level, the first with a positive slope and the second with a negative slope). During a separation interval, log(*Ni/Ns*) is above the selected level. Thus, the two separations between the three depletions are approximately equal to 30 s and 225 s. For each level, duration and separation bins can be associated with their corresponding numbers in histograms.

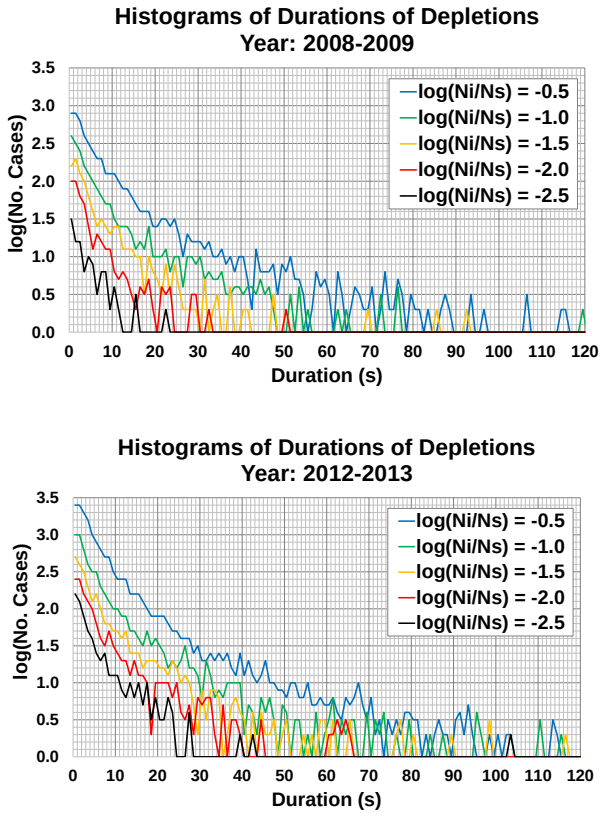

Figure 6. Histograms of duration of depletions for the five log(Ni/Ns) levels and the entire data set of C/NOFS PLP ion density data corresponding to each of the two different years (upper panel: 01 October 2008 to 30 September 2009; and lower panel: 05 June 2012 to 04 June 2013). The first year corresponds to solar minimum conditions and the second one is as close to solar maximum conditions of solar cycle 24 as possible at the time of the analysis.

The analysis just described has been applied to the curves log(*Ni/Ns*) corresponding to the evening-hours sections of all C/NOFS satellite orbits, for each of the five levels and each year. Thus, the analysis is based on curves that are similar to but longer than the red curve displayed in Figure 3, which is limited to a 15-min record.

The histograms for the durations of depletions at the five different log(*Ni/Ns*) levels during the two different years are shown in Figure 6. It is observed that, in the log-log scale of Figure 6, the numbers of cases decrease linearly with duration, for values of the latter that are less than approximately 20 s, regardless of the log(*Ni/Ns*) levels. For longer durations, the numbers of cases corresponding to the three lower log(*Ni/Ns*) levels decrease more slowly than initially. The average numbers of short-duration depletions (less than 40 s), which are well represented by all histograms, increase by factors between 2.5 and 3.5 from 2008-2009 to 2012-2013.

The histograms for the separations between consecutive depletions at the five different log(*Ni/Ns*) levels during the two different years are shown in Figure 7.

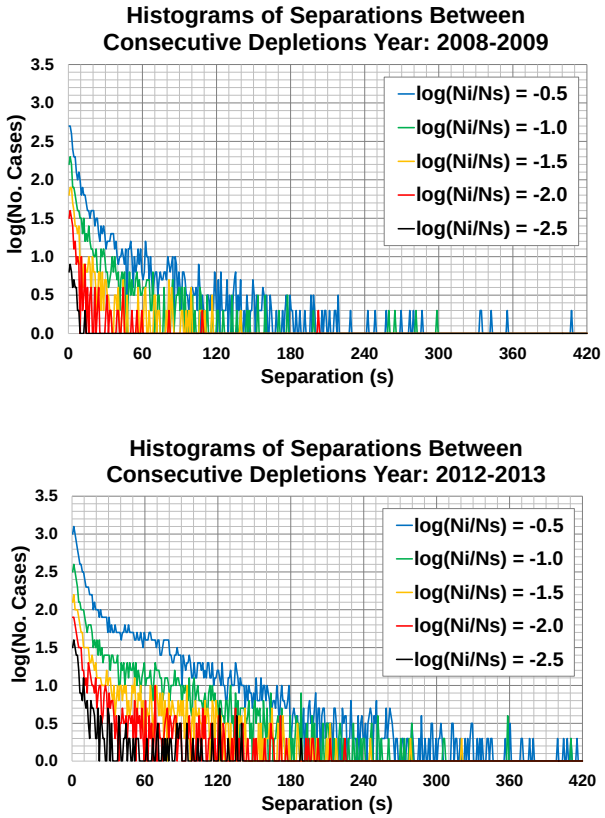

Figure 7. Histograms of separations between depletions for the five log(Ni/Ns) levels and the entire data set of C/NOFS PLP ion density data corresponding to each of the two different years (upper panel: 01 October 2008 to 30 September 2009; and lower panel: 05 June 2012 to 04 June 2013). The first year corresponds to solar minimum conditions and the second one is as close to solar maximum conditions of solar cycle 24 as possible at the time of the analysis.

It is observed that the general behavior of the separation between consecutive depletions follows that of the duration, as described above. However, it is also observed that the separation extends to longer time intervals than those of the duration, for the same log(*Ni/Ns*) level.

Conclusions

The present contribution has shown that the number, durations and separations of equatorial plasma bubbles depends on solar activity. It is also important to note that the separation between consecutive depletions extends to longer time intervals than those of the duration

Acknowledgments

This material is based upon work supported by the Air Force Office of Scientific Research under award number FA9550-16-1-0377.

References

1. W. J. Burke, C. Y. Huang, L. C. Gentile, and L. Bauer, "Seasonal-Longitudinal Variability of Equatorial Plasma Bubbles," *Annales Geophysicae*, **22**, September 2004, pp. 3089–3098, doi: 10.5194/angeo-22-3089-2004.

2. C. Y. Huang, W. J. Burke, J. S. Machuzak, L. C. Gentile, and P. J. Sultan, "Equatorial Plasma Bubbles Observed by DMSP Satellites During a Full Solar Cycle: Toward a Global Climatology," *Journal of Geophysical Research*, **107**, A12, December 2002, pp. 1434-1443, doi: 10.1029/2002JA009452.

3. Y. Kil and R. A. Heelis, "Global Distribution of Density Irregularities in the Equatorial Ionosphere," *Journal of Geophysical Research*, **103**, A1, January 1998, pp. 407–417, doi: 10.1029/97JA02698.

4. S.-Y. Su, C. H. Liu, H. H. Ho, and C. K. Chao, "Distribution Characteristics of Topside Ionospheric Density Irregularities: Equatorial Versus Midlatitude Regions," *Journal of Geophysical Research*, **111**, A6, June 2006, pp. A06305_1- A06305_17, doi: 10.1029/2005JA011330, 2006.

5. J. P. McClure, W. B. Hanson, and J. H. Hoffman, "Plasma Bubbles and Irregularities in the Equatorial Ionosphere," *Journal of Geophysical Research*, **82**, 19, July 1977, pp. 2650-2656, doi: 10.1029/JA082i019p02650.

6. G. Le, C.-S. Huang, R. F. Pfaff, S.-Y. Su, H.-C. Yeh, R. A. Heelis, F. J. Rich, and M. Hairston, "Plasma Density Enhancements Associated with Equatorial Spread *F*: ROCSAT-1 and DMSP Observations," *Journal of Geophysical Research*, **108**, A8, August 2003, pp. 1318_1-1318_14, doi:10.1029/2002JA009592.

7. C.-S. Huang, G. Le, O. de La Beaujardiere, P. A. Roddy, D. E. Hunton, R. F. Pfaff, and M. R. Hairston, Relationship between plasma bubbles and density enhancements: Observations and interpretation, *Geophysical Research*, **119**, A2, February 2014, pp. 1325–1336, doi:10.1002/2013JA019579.

8. C.-S. Huang, O. de La Beaujardiere, P. A. Roddy, D. E. Hunton, J. Y. Liu, and S. P. Chen (2014), "Occurrence Probability and Amplitude of Equatorial Ionospheric Irregularities Associated with Plasma Bubbles During Low and Moderate Solar Activities (2008–2012)," *Journal of Geophysical Research*, **119**, A2, February 2014, pp. 1186–1199, doi:10.1002/2013JA019212.

9. E. Costa, E., P. A. Roddy, and J. O. Ballenthin, "Statistical Analysis of C/NOFS Planar Langmuir Probe Data," Annales Geophysicae, **32**, 7, July 2014, pp. 773-791, doi:10.5194/angeo-32-773-2014.